Int. J. Heat Mass Transfer. Vol. 22, pp. 885–899
Pergamon Press Ltd. 1979. Printed in Great Britain

TURBULENT HEAT AND MASS TRANSFERS ACROSS A ROUGH, AIR–WATER INTERFACE: A SIMPLE THEORY

ROBERT L. STREET*
Department of Civil Engineering, Stanford University, Stanford, CA 94305, U.S.A.

(*Received* 17 *October* 1977 *and in revised form* 28 *July* 1978)

Abstract—The net transfer across an air–water interface depends on heat transfer in the aqueous surface layer, radiation at the interface, and sensible heat and water vapor transfers in the air surface layer. The coupled problem for this net transfer across an interface under the action of a turbulent air flow is solved by application of a theory for rough wall flows. Theoretical predictions and data obtained in a laboratory facility are in quantitative agreement. Prediction of transfers and interface temperature is made from knowledge of the interface shear stress and mean roughness height plus temperature and humidity at a point in the air surface layer and the temperature at a point in the water surface layer.

NOMENCLATURE

c_p, heat capacity (specific heat at constant pressure) [$J\,kg^{-1}\,K^{-1}$];
D, molecular mass diffusivity of water vapor in air [$m^2\,s^{-1}$];
E, emissivity of radiation;
H, humidity [kg vapor/kg dry air];
h, mean roughness (wave) height [m];
$\bar{h}$, mean height of high frequency components [22] [m];
h_p, representative rms height corresponding to peak of frequency distribution of local scale height [22] [m];
K, effective diffusivity [$m^2\,s^{-1}$];
k', von Karman constant;
L, latent heat of vaporization for water [$J\,kg^{-1}$];
L_0, Monin–Obukhov length; approaches ∞ for neutrally stable flows considered herein [m];
l, mixing length or scale of turbulent eddies [m];
Pr, ν/κ; Prandtl number;
Pr_t, $\varepsilon_M/\varepsilon_H$; turbulent Prandtl number;
Q_L, latent heat transfer at the interface [$W\,m^{-2}$];
Q_R, net radiation flux from the interface [$W\,m^{-2}$];
Q_S, sensible heat flux in the air [$W\,m^{-2}$];
Q_T, total heat flux = heat flux in water surface layer [$W\,m^{-2}$];
Q_V, water vapor flux in the air [$kg\,m^{-2}\,s$];
q, specific humidity [kg vapor/kg mixture];
q_s, interface specific humidity;
Re_{δ_v}, Reynolds number $= \delta_v U(\delta_v)/\nu$;
Sc, ν_a/D; Schmidt number;
Sc_t, $\varepsilon_M/\varepsilon_E$; turbulent Schmidt number;
St_a, heat transfer Stanton number in air;
St_e, latent heat transfer Stanton number at interface;
St_m, water vapor mass-transfer Stanton number;
St_w, heat transfer Stanton number in water;
T_s, interface temperature [°C];
$U(z)$, horizontal component of the velocity [$m\,s^{-1}$];
u_*, $(\tau_0/\rho)^{1/2}$; friction velocity [$m\,s^{-1}$];
$(\overline{u'^2})^{1/2}, (\overline{w'^2})^{1/2}$, root-mean-square velocity fluctuations in horizontal and vertical directions, respectively;
x, streamwise distance (fetch) from start of boundary layers [m];
z, vertical coordinate; measured positive upwards from mean interface level [m];
z_0, wall roughness parameter [m].

Greek symbols

β_S, Q_S/Q_L; Bowen ratio;
ΔT, $T_b - T_\infty$; water–air temperature difference [°C];
δ_Q, δ_T, matched layer thicknesses [m];
δ_q, δ_t, sublayer thicknesses [m];
δ_v, viscous sublayer thickness [m];
ε_E, water vapor (mass) eddy diffusivity [$m^2\,s^{-1}$];
ε_H, thermal eddy viscosity [$m^2\,s^{-1}$];
ε_M, eddy viscosity [$m^2\,s^{-1}$];
η, displacement of interface from the mean level [m];
κ, molecular thermal diffusivity [$m^2\,s^{-1}$];
ν, kinematic viscosity [$m^2\,s^{-1}$];
ρ, density [$kg\,m^{-3}$];
σ, Stefan–Boltzmann constant [$5.673 \times 10^{-8}\,W\,m^{-2}\,K^{-4}$];
τ_0, shear stress at the interface [$kg\,m^{-1}\,s^{-2}$];
Φ_H, Φ_E, dimensionless gradients; equal Pr_t and Sc_t when the Monin–Obukhov length $L_0 \to \infty$.

*Senior Postdoctoral Fellow (1978), National Center for Atmospheric Research, Boulder, Colorado 80307, U.S.A.

The national Center for Atmospheric Research is sponsored by the National Science Foundation.

Subscripts

- a, air surface layer;
- b, quantity measured in bulk or fully turbulent portion of water stream at depth $|z_b|$;
- Q,q, water–vapor-related property in air;
- T,t, thermal or heat-transfer-related property;
- w, water surface layer.

Superscript

- $+$, dimensionless (Reynolds) numbers, e.g. $h^+ = u_* h/\nu$.

1. INTRODUCTION

MANY papers have been written about transfers across an air–water interface. With the single exception of Kotake [1, 2], who solved laminar flow systems, all have been focused on either the air or the aqueous surface layers. Thus, the coupled surface layer transport problem remains unsolved for turbulent flow conditions. However, the turbulent flow conditions are important for a range of engineering and geophysical applications where a phase-changing interface is involved.

In Street and Miller [3] the theory of rough-wall flows was applied to obtain the thickness of the viscous and thermal sublayers in the water beneath an air–water interface. In the present paper the concepts outlined in [3] are applied to both the air and water surface layers and the resulting transport estimates are summed to obtain the total transport in each layer. The interface temperature T_s is then obtained under the constraint that the total transfer through the aqueous layer equal the sum of the radiation and latent heat transfer at the interface plus the sensible heat transfer through the air surface layer. The result is a tool for quantitative prediction of the sensible, latent and total heat and mass transfers in the surface layers at a rough air–water interface.

2. PREVIOUS WORK

2.1. *The aqueous surface layer*

Saunders [4] gave a simple theory which related the surface-water/bulk-water temperature difference at the ocean–air interface to the heat transfer and the stress on the interface. His theory is based on the concept that the majority of the temperature variation in the aqueous surface layer occurs within a region where the flux of heat is transmitted principally by molecular conduction.

Hasse [5] determined the temperature difference across the aqueous surface layer as a function of total heat flux through the layer by use of the fundamental equation for heat transfer in the water and wind tunnel determinations of the effective thermal diffusivity in a turbulent boundary layer. The evaluation of his diffusivity equation did not require knowledge of the thermal or viscous sublayer thicknesses but, rather, Hasse employed an empirical diffusivity relationship derived for solid boundaries and assumed to be correct through the entire water surface layer.

Yaglom and Kader [6] and Owen and Thomson [7] discussed flow over and heat transfer from rough surfaces. They envisioned a region of molecularly dominated flow around and between the roughness elements with turbulent flow outside this region. Working from the concepts of Yaglom and Kader [6] to obtain expressions for the eddy diffusivities for heat and momentum and from Hasse's [5] surface layer heat flux equation, Street and Miller [3] determined the aqueous sublayer thicknesses at rough air–water interface.

Kondo [8] proposed a hypothesis of hydrodynamic similarity for both the air and aqueous boundary layers adjoining an air–water interface. Both layers were combined through an identical geometric roughness height which is presumed to be composed of the high-frequency components of the waves on the interface. The hypothesis was then applied to the aqueous surface layer. The hydrodynamic roughness length and the thermometric and mass transport coefficients were obtained in terms of the roughness Reynolds number based on the geometric roughness height. Transport was predicted from known values of the surface stress and either the temperatures or concentrations at the interface and at some depth in the aqueous surface layer. Significantly, Kondo's [8] excellent results are based on a hypothesis involving purely turbulent fluids without any consideration of a direct contribution due to the orbital motions of the water waves.*

Indeed, using the high-frequency components of the surface wave spectrum as a measure of roughness, he treated the interface as though it were a solid boundary for both the air and the aqueous surface layer flows.

2.2. *The air surface layer*

Brutsaert [9] outlined a theory for evaporation into or heat transfer through the air surface layer. His formulation recognized the need to account for molecular domination of the transfer near solid boundaries or interfaces and adopted a surface renewal model (see Davies [10] for a complete discussion of surface renewal models) near the interface. In his comparison with experimental data, Brutsaert used, among others, the data set of Mangarella *et al.* [11]. These data exhibit behavior consistent with Brutsaert's rough wall theory and are noted here because key results from the Mangarella *et al.* [11] (see also Mangarella *et al.* [12]) data set are employed in this paper.

Kondo [13] estimated the bulk transfer coefficients associated with the sea surface by use of data

*Preliminary data taken in the Stanford laboratory facility and using a laser-Doppler anemometer and high-speed thermistor confirm that the wave orbital motions make no direct contribution to the aqueous surface layer heat flux.

for the roughness Reynolds number of the interface and the Owen and Thomson [7] theory for transfer from a rough surface to the air flow above it. Prediction of the transfers of heat and water vapor are made from knowledge of the surface temperature and specific humidity, the air temperature and specific humidity at a point in the air surface layer, the surface shear stress and the wave characteristics (expressed in terms of a representative surface roughness height).

2.3. *Coupled surface layers*

Kotake [1] studied gas and liquid laminar flows having a phase-changing (evaporation or condensation) interface at their common boundary assuming constant fluid properties and a flat surface with zero pressure gradient. He noted that a preliminary and fundamental approach to such a problem is a study under the condition that the quantities at the interface are given explicitly. With regard to energy transfer, all studies cited above followed this approach. Kotake points out, however, that for two-layer flows of a gas and a liquid which have an appreciable velocity at the interface to force the liquid into motion, or which have a large gradient of temperature in the liquid layer, the boundary conditions at the interface should be provided implicitly through the continuity relationships for mass, momentum and energy fluxes across the interface between layers. This concept provides the basis of the present analysis.

Kotake [2] followed up on his first paper and studied gas and liquid laminar flows having a wavy phase-changing interface. He studied analytically the features of the wave-induced disturbances. The present paper does not follow this approach, taking rather a simpler view of the mean flow conditions for a turbulent flow.

3. THEORETICAL FOUNDATIONS

This analysis parallels and extends that in [3]; accordingly all the arguments given there are not repeated here. This section begins with a brief review of [3]; then the present theory is formulated in two parts, the first being a flux formulation with account for the flow characteristics and the second a formulation of the equality-of-flux constraint.

3.1. *Review*

Using the air-surface layer data of Mangarella *et al.* [11] and Chambers *et al.* [14], Miller *et al.* [15] created a smoothed set of sensible and latent heat transfer coefficients for the full range of water–air temperature differences and air speeds at two measurement stations used in the Stanford Wind, Water Wave Research Facility. They then measured the near-surface water temperature, the bulk water temperature, the interface characteristics, and mean air-flow data, the last being necessary to use the smoothed transfer coefficient data.

Street and Miller [3] derived theoretical relations between the dimensionless heat-transfer coefficient for the aqueous surface layer and the thermal sublayer thickness in the case of flow past a fully rough boundary. This thickness is proportional to the square root of the mean interface roughness height h and to the inverse of the one-third power of the molecular Prandtl number Pr, and is dependent on the shape of the roughness elements. Using a limited sample of the experimental data in [15], viz. cases with water–air temperature differences of about 2 1/2, 5 and 7 1/2 C and air speeds of 7 1/2 and 10 m s^{-1} at fetches (distance from the facility air flow inlet) of 9.5 and 14.5 m, Street and Miller [3], first, found the dimensionless aqueous surface layer heat-transfer coefficient by use of the smoothed Mangarella *et al.* data and measured the mean flow conditions and, then, inferred the proportionality constant in the sublayer thickness relationship for fully rough flows.

Although the above result was derived solely from heat transfer data, it is convenient to express the result in terms of the viscous sublayer thickness, the relationship between viscous and thermal sublayer thicknesses having been shown in [3] to be a consequence of the definition of rough flow character (cf. [6]) and independent of the turbulent characteristics of the flow away from the boundary. The key results of [3] are that the dimensionless viscous and thermal sublayer thicknesses in the water, $\delta^+_{v_w}$ and $\delta^+_{t_w}$ respectively (see detailed definitions below), are related by:

$$\delta^+_{t_w}/\delta^+_{v_w} = Pr^{-1/3} \tag{1}$$

and are related to the dimensionless mean roughness height h^+_w by:

$$\delta^+_{v_w} = Pr^{1/3}\delta^+_{t_w} = 0.37(h^+_w)^{1/2}. \tag{2}$$

While the constant 0.37 was inferred from experimental data, the form of equation (2) arises solely from the dimensional and physical argument (see [6]) that the Reynolds number $Re_{\delta_{v_w}}$ at the edge of the viscous sublayer, viz.,

$$Re_{\delta_{v_w}} = \delta_{v_w} U_w(\delta_{v_w})/\nu_w, \tag{3}$$

be of order one, indicating the dominance of molecular action.

The essence of the present development is that the relationships in equations (1) and (2) should be universal for all rough wall flows, apart from possible effects on the proportionality constant 0.37 caused by roughness shape (cf. [6] or [7]). Indeed, by comparing the results of [3] and [6] one can deduce that, at least for $Pr \gg 1$, the proportionality constant 0.46 (corresponds to the selected $b'_1 = 0.55$ in [6]) fits a significant portion of the solid, rough wall data, which was obtained over markedly different roughness shapes (essentially more angular) than those presented by water waves. Because the roughness shapes are identical for the air and water surface layers on opposite sides of an interface it is logical to use the relationship (2) for analysis of rough-wall flows in both layers.

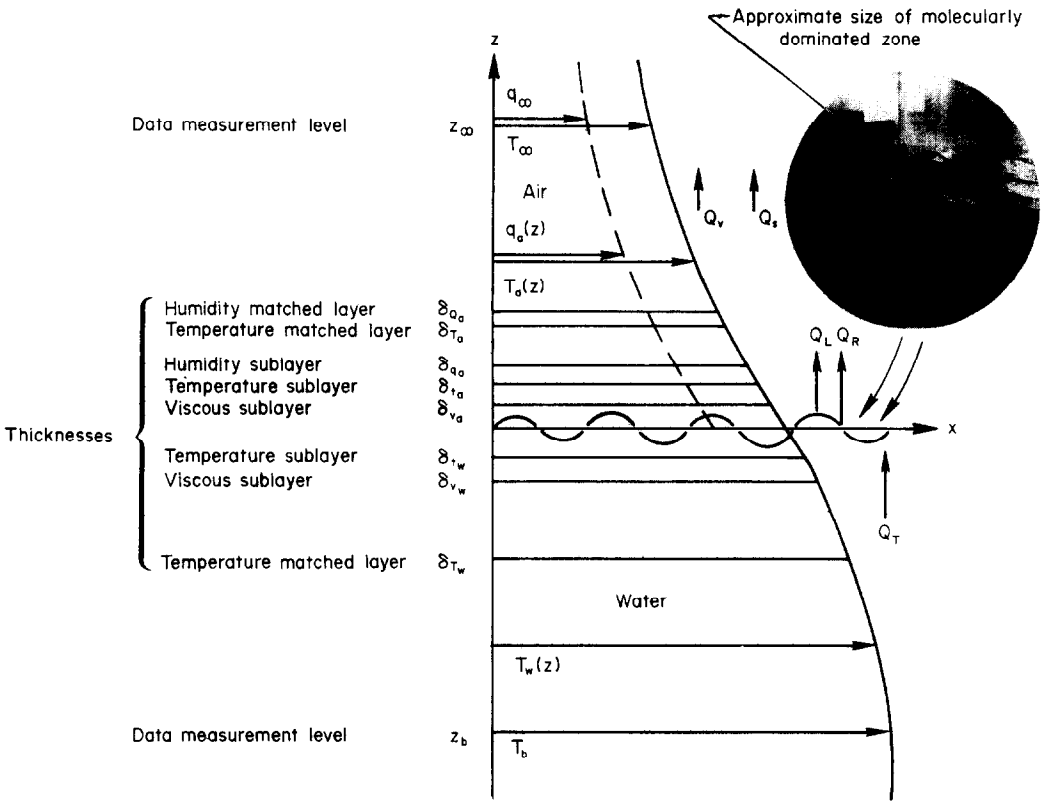

FIG. 1. Schematic of the surface layers at an air–water interface.

3.2. *Development of flux equations*

Figure 1 is a schematic of the surface layers at a rough air–water interface. Consider fully-developed horizontal streams of an incompressible gas (air) moving over a liquid (water), i.e. variations in properties with respect to streamwise distance or fetch (x) are negligible. Let the flow be steady in the mean; then,

$$Q_T = -\rho_w c_{p_w} k_w \frac{dT_w}{dz}, \tag{4}$$

$$Q_S = -\rho_a c_{p_a} K_a \frac{dT_a}{dz}, \tag{5}$$

$$Q_V = -\rho_a K_q \frac{dq_a}{dz}, \tag{6}$$

in the surface layers, while at the interface:

$$Q_R = E_w \sigma (T_{SABS}^4 - E_a T_{\infty ABS}^4) \tag{7}$$

$$Q_L = L Q_V. \tag{8}$$

In these equations, Q_T is the total flux (positive upward) and the heat flux in the water surface layer, Q_S is the sensible heat flux in the air, Q_V is the water vapor flux in the air, Q_R is the net radiation flux from the interface, and Q_L is the latent heat transfer at the interface. In the surface layers Q_T, Q_S and Q_V are assumed to be constant; Q_R is assumed to come from an infinitesimal layer at the interface. The particular form of equation (4) is selected for ease in interpretation of our laboratory data; other forms would be appropriate for other applications. For the purposes of this analysis, only long-wave radiation from the surroundings and the water surface is accounted for. Thus, equation (7) represents the net long-wave back radiation from the interface ($E_w \sigma T_{SABS}^4$) less the incoming long-wave radiation (solar or short-wave radiation is not present in the laboratory) from the surroundings, e.g. the air ($E_a \sigma T_{aABS}^4$), plus that fraction of the surrounding radiation which is reflected (not absorbed) from the interface $[E_a \sigma T_{aABS}^4 (1 - E_w)]$.

The remaining variables in equations (4)–(8) are the density of water and air (ρ_w and ρ_a), the heat capacity of water and air (c_{p_w} and c_{p_a}), the latent heat of vaporization L for water, the emissivity of water and air (E_w and E_a), the Stefan–Boltzmann constant σ, the specific humidity of the air q_a, the air and water temperatures (T_a and T_w) and the effective diffusivities $K_a(z)$, $K_w(z)$ and $K_q(z)$. The coordinate z is measured positive upward from the mean interface level.

If temperature and humidity effects on both the fluid densities or heat capacities are ignored, equations (4), (5) and (8) can be rewritten:

$$dT_w = \left(\frac{-Q_T}{\rho_w c_{p_w}}\right) \frac{dz}{K_w(z)} \tag{9}$$

$$dT_a = \left(\frac{-Q_S}{\rho_a c_{p_a}}\right) \frac{dz}{K_a(z)} \tag{10}$$

$$dq_a = \left(\frac{-Q_L}{\rho_a L}\right) \frac{dz}{K_q(z)}. \tag{11}$$

The essence of the method used herein is to apply the concepts of rough-wall boundary-layer theory [3] to define the diffusivities for heat (K_w and K_a) and water vapor (K_q) and then to integrate equations (9)–(11). The region of molecularly dominated flow lies around and between the roughness protuberances (Yaglom and Kader [6]) which in this case are the surface water waves. As noted above, dimensional arguments allow definition of molecularly-dominated sublayers within the surface layers with thicknesses of the order of the square root of the roughness Reynolds number based on the mean wave height (in a more general context, this height should be the mean height of the high frequency components [8, 13]).

To define K_a, K_w and K_q the viscous, thermal and water vapor (humidity) sublayers must be described. In Fig. 1 are shown:

(1) Viscous sublayers of thicknesses δ_{v_a} and δ_{v_w} in which the molecular viscosity v_a or v_w dominates the eddy viscosity ε_M; $\varepsilon_M(\delta_v) = v$.

(2) Thermal sublayers of thicknesses δ_{t_a} and δ_{t_w} in which the thermal molecular diffusivity κ_a or κ_w dominates the eddy diffusivity for heat ε_H; $\varepsilon_H(\delta_t) = \kappa$.

(3) A humidity or water vapor sublayer in the air of thickness δ_{q_a} in which the molecular mass diffusivity for water vapor D dominates the eddy diffusivity for water vapor ε_E; $\varepsilon_E(\delta_q) = D$.

(4) A set of matched layers at $z = -\delta_{T_w}$, δ_{T_a}, δ_{Q_a}, where the eddy diffusivities become equal to a value appropriate to a logarithmic variation of temperature or humidity in a turbulent boundary layer.

From these definitions and [3], the necessary expressions are obtained. First, the following Reynolds number forms are defined; for an air quantity, say the measurement level z_∞, $z_\infty^+ = u_{*a} z_\infty / v_a$, and for a water quantity, say the measurement level z_b, $z_b^+ = u_{*w} z_b / v_w$. Similarly, $\delta_{t_a}^+ = u_{*a}\delta_{t_a}/v_a$, etc. Here $u_{*a} = (\tau_0/\rho_a)^{1/2}$ and $u_{*w} = (\tau_0/\rho_w)^{1/2}$ are the friction velocities in the air and water surface layers for an assumed constant shear stress τ_0 (see Section 4 for a discussion of appropriate u_* values). Second, the key result from [3], viz., equation (2) is employed; there, $h^+ = u_* h/v$ where, for the present laboratory data, h is the mean roughness height at the interface (see Section 4). This result is applied now to both the air and water layers (with appropriate subscripts). Next the effective diffusivity expressions are written. For these, the eddy diffusivities within the sublayers and matched layers are assumed to vary with the cube of distance from the interface (cf. [3] or [6]).

This assumed variation of the eddy diffusivities with the cube of the distance from the interface needs some examination (see, e.g. [16]). It is typical to define eddy viscosities or diffusivities in the form

$$\varepsilon \sim (\overline{w'^2})^{1/2} l$$

where $(\overline{w'^2})^{1/2}$ is the root-mean-square vertical velocity fluctuation and l is the mixing length or eddy size (i.e. a measure of the scale of the turbulent eddies). The actual variation of ε with distance from a boundary or interface depends then on how $(\overline{w'^2})^{1/2}$ and l vary with distance.

Levich [17] and Davies [10] distinguish between flow past solid boundaries and flow of a liquid at a so-called "clean" gas–liquid interface, a clean interface being defined specifically by Davies [10, pp. 175 and 250] as an interface at which there is no surface film and no tangential stress. Near a solid boundary where there is a shear stress and the no-slip condition applies, the horizontal component of the velocity of eddies, i.e. $(\overline{u'^2})^{1/2}$, varies linearly with distance from the boundary. Application of the continuity equation shows that the normal (or vertical) component of this velocity, i.e. $(\overline{w'^2})^{1/2}$, must then vary as the square of the distance. If the scale of eddy motion is taken (as usual) to vary linearly with distance from the boundary, the eddy diffusivities must vary as the cube of the distance. This relation is used by Yaglom and Kader [6] for flow past rough solid boundaries.

However, in the analyses by Levich [17] and Davies [10] of a "clean" surface, the tangential stress is zero. As a consequence $(\overline{u'^2})^{1/2}$ does not vary with distance from the interface; $(\overline{w'^2})^{1/2}$ therefore varies linearly, and the eddy diffusivities vary only as the square of distance from the boundary.

For solid boundaries Yaglom and Kader [6] cite ample evidence for employing the cubic estimate. The cubic variation also appears reasonable for the air flow because the ratio of air to water densities ($\sim 1/800$) suggests that the water boundary appears relatively solid to the air flow. The theory of Brutsaert [9] which was applied to Stanford facility data (see Section 2.2) also confirms the appropriateness of treating the water interface as a solid rough surface.

The large ratio of water-to-air densities suggests that the air cannot restrict water motions in the same manner as the water restricts air motions, although eddy-induced vertical motions are strongly damped by surface tension and gravitational action. On the other hand, in the present cases (with a high air speed) the air stream imposes a sizeable shear stress on the water, leading to wave (roughness) growth with fetch (x) and generation of a turbulent surface layer current [18]. Thus, the air–water interface is not a "clean" interface in the sense described above, but is a stressed interface. At a stressed interface the horizontal velocity fluctuations in an eddy approaching the interface will be damped by the effect of the stress much as in the cases of solid boundaries or film-covered interfaces. Accordingly, the variation of eddy (i.e. root-mean-square) velocities and scales near the stressed interface must be more similar to those described above for a solid surface than to those near a mobile, but unstressed interface. The results of Kondo [8] and Wu [19] also support the contention that the water surface layer flow acts similar to flow past a solid boundary.

Street and Miller [3] used the cubic variation of the eddy diffusivities appropriate to solid boundaries and their results demonstrate precisely the behavior predicted for flow past a rough boundary, i.e. the sublayer thicknesses are proportional to $(h_w^+)^{1/2}$ and $Re_{\delta_{v_w}} = O(1)$ for $h_w^+ > 100$ [cf., equations (2) and (3)]. Actually, for their results and from equations (2) and (3):

$$Re_{\delta_{v_w}} \sim (\delta_{v_w}^+)^2/h_w^+ = (0.37)^2 = 0.14,$$

because (cf. [6]) $U(\delta_{v_w}) \sim u_{*_w}\delta_{v_w}/h_w$. From Section 3.1 one can infer that $Re_{\delta_v} \sim 0.21$ for flow past a solid rough boundary.

On the other hand it is a simple matter to rederive the results of Street and Miller [3] for the case of an unstressed interface, i.e. with $\varepsilon \sim z^2$. Among other results this yields:

$$\delta_{t_w}^+/\delta_{v_w}^+ = Pr^{-1/2},$$

[cf. equation (1)] and a new expression relating the dimensionless heat-transfer coefficient and $\delta_{t_w}^+$. Using the Street and Miller data for $h_w^+ > 100$ yields

$$\delta_{t_w}^+ Pr^{1/2} = \delta_{v_w}^+ = (0.14 \pm 0.02)(h_w^+)^{1/2}$$

and $Re_{\delta_{v_w}} \sim (0.14)^2 = 0.02 \neq O(1)$. Thus, while this new approach obtains the proportionality to $(h_w^+)^{1/2}$ at about the same accuracy as the cubic estimate, the requirement that $Re_{\delta_v} \sim O(1)$ is not satisfied.

In view of the above discussion and results, the cubic variation of eddy diffusivity is used as in Street and Miller [3] and the result is

(1) In the water surface layer:

$$K_w(z^+) = \begin{cases} \kappa_w[1-(z^+/\delta_{t_w}^+)^3], & z^+ > -\delta_{T_w}^+ \\ \kappa_w[1-k'Pr_w z^+/Pr_{t_w}], & z^+ \leqslant -\delta_{T_w}^+, \end{cases} \tag{12}$$

where $z^+ \leqslant 0$, k' is the von Karman constant taken to be 0.40, $Pr_w = \nu_w/\kappa_w$ is the molecular Prandtl number for water, and $Pr_{t_w} = \varepsilon_{M_w}/\varepsilon_{H_w}$ is the turbulent Prandtl number. In the present analysis the ratio of eddy viscosity ε_{M_w} to eddy diffusivity ε_{H_w} is allowed to be different from unity in the fully turbulent portion of a profile (where $z^+ < -\delta_{T_w}^+$ for example). Thus, at the matched layer the cubic estimate for $\varepsilon_{H_w}\{\sim (z^+)^3$ when $z^+ \geqslant -\delta_{T_w}^+\}$ is matched to the turbulent estimate:

$$\varepsilon_{H_w} = \frac{\varepsilon_{M_w}}{Pr_{t_w}} = k'u_{*_w}z/Pr_{t_w}, \quad z \leqslant -\delta_{T_w}.$$

The appropriate sublayer thicknesses are [3]:

$$\delta_{t_w}^+ = Pr_w^{-1/3}\delta_{v_w}^+ \tag{13}$$

$$\delta_{T_w}^+ = (k'/Pr_{t_w})^{1/2}(\delta_{v_w}^+)^{3/2}. \tag{14}$$

(2) In the air surface layer (following the same pattern as in the water):

$$K_a(z^+) = \begin{cases} \kappa_a[1+(z^+/\delta_{t_a}^+)^3], & z^+ < \delta_{T_a}^+ \\ \kappa_a[1+k'Pr_a z^+/Pr_{t_a}], & z^+ \geqslant \delta_{T_a}^+ \end{cases} \tag{15}$$

$$K_q(z^+) = \begin{cases} D[1+(z^+/\delta_{q_a}^+)^3], & z^+ < \delta_{Q_a}^+ \\ D[1+k'Sc_a z^+/Sc_{t_a}], & z^+ \geqslant \delta_{Q_a}^+. \end{cases} \tag{16}$$

Here, Pr_a and Pr_{a_t} are the molecular and turbulent Prandtl numbers for air, while $Sc_a = \nu_a/D$ and $Sc_{t_a} = \varepsilon_{M_a}/\varepsilon_{E_a}$ are the molecular and turbulent Schmidt numbers for water vapor. According to the pattern for the water surface layer, the appropriate sublayer thicknesses in the air surface layer are [cf. equations (13) and (14)]:

$$\delta_{t_a}^+ = Pr_a^{-1/3}\delta_{v_a}^+ \tag{17}$$

$$\delta_{T_a}^+ = (k'/Pr_{t_a})^{1/2}(\delta_{v_a}^+)^{3/2} \tag{18}$$

$$\delta_{q_a}^+ = Sc_a^{-1/3}\delta_{v_a}^+ \tag{19}$$

$$\delta_{Q_a}^+ = (k'/Sc_{t_a})^{1/2}(\delta_{v_a}^+)^{3/2}. \tag{20}$$

Equations (12), (15) and (16) are next introduced into equations (9)–(11) which are integrated from the mean water level ($z^+ = 0$) to the appropriate data measurement level (i.e. the points in the surface layers at which the air temperature and humidity and the bulk water temperature are measured so that the fluxes and surface temperature T_s can be predicted). The results are:

$$T_b - T_s = \left(\frac{Q_T \nu_w}{\rho_w c_{p_w} u_{*_w}}\right) \int_{z_b^+}^{0} \frac{dz^+}{K_w(z^+)}$$

$$T_s - T_\infty = \left(\frac{Q_S \nu_a}{\rho_a c_{p_a} u_{*_a}}\right) \int_{0}^{z_\infty^+} \frac{dz^+}{K_a(z^+)}$$

$$q_s - q_\infty = \left(\frac{Q_L \nu_a}{\rho_a L u_{*_a}}\right) \int_{0}^{z_\infty^+} \frac{dz^+}{K_q(z^+)},$$

or:

$$1.\quad Q_T = \rho_w c_{p_w} u_{*_w}(T_b - T_s)St_w, \tag{21}$$

where $St_w = Q_T/\rho_w c_{p_w} u_{*_w}(T_b - T_s)$ is the Stanton number for heat flux in the aqueous surface layer (Kondo [8, 13] defines the inverse of the Stanton number to be a generalized transfer resistance).

Thus:

$$\frac{1}{St_w} = \nu_w \int_{z_b^+}^{0} \frac{dz^+}{K_w(z^+)} = \frac{Pr_w \delta_{t_w}^+}{3}\left\{\tfrac{1}{2}\ln\left[\frac{(\delta_{t_w}^+ + \delta_{T_w}^+)^2}{(\delta_{t_w}^{+2} - \delta_{t_w}^+\delta_{T_w}^+ + \delta_{T_w}^{+2})}\right] + (3)^{1/2}\left[\tan^{-1}\frac{2\delta_{T_w}^+ - \delta_{t_w}^+}{(3)^{1/2}\delta_{t_w}^+} + \tan^{-1}(3)^{-1/2}\right]\right\} + \frac{Pr_{t_w}}{k'}\ln\left\{\frac{1-k'Pr_w z_b^+/Pr_{t_w}}{1+k'Pr_w\delta_{T_w}^+/Pr_{t_w}}\right\} \tag{22}$$

$$2.\quad Q_S = \rho_a c_{p_a} u_{*_a}(T_s - T_\infty)St_a, \tag{23}$$

where $St_a = Q_S/\rho_a c_{p_a} u_{*_a}(T_s - T_\infty)$ and

$$\frac{1}{St_a} = \nu_a \int_{0}^{z_\infty^+} \frac{dz^+}{K_a(z^+)} = \frac{Pr_a \delta_{t_a}^+}{3}\left\{\tfrac{1}{2}\ln\left[\frac{(\delta_{t_a}^+ + \delta_{T_a}^+)^2}{(\delta_{t_a}^{+2} - \delta_{t_a}^+\delta_{T_a}^+ + \delta_{T_a}^{+2})}\right] + (3)^{1/2}\left[\tan^{-1}\frac{2\delta_{T_a}^+ - \delta_{t_a}^+}{(3)^{1/2}\delta_{t_a}^+} + \tan^{-1}(3)^{-1/2}\right]\right\} + \frac{Pr_{t_a}}{k'}\ln\left\{\frac{1+k'Pr_a z_\infty^+/Pr_{t_a}}{1+k'Pr_a\delta_{T_a}^+/Pr_{t_a}}\right\} \tag{24}$$

$$3.\quad Q_L = \rho_a L u_{*a}(q_s - q_z)St_e, \tag{25}$$

where $St_e = Q_L/\rho_a L u_{*a}(q_s - q_z)$ and

$$\frac{1}{St_e} = v_a \int_0^{z_z^+} \frac{dz^+}{K_q(z^+)} = \frac{Sc_a \delta_{qa}^+}{3}\left\{\tfrac{1}{2}\ln\left[\frac{(\delta_{qa}^+ + \delta_{Qa}^+)^2}{(\delta_{qa}^{+2} - \delta_{qa}^+\delta_{Qa}^+ + \delta_{Qa}^{+2})}\right] + (3)^{1/2}\left[\tan^{-1}\frac{2\delta_{Qa}^+ - \delta_{qa}^+}{(3)^{1/2}\delta_{qa}^+} - \tan^{-1}(3)^{-1/2}\right]\right\} + \frac{Sc_{ta}}{k'}\ln\left\{\frac{1 + k'Sc_a z_z^+/Sc_{ta}}{1 + k'Sc_a\delta_{Qa}^+/Sc_{ta}}\right\}. \tag{26}$$

The mass transfer Stanton number $St_m = Q_V/\rho_a u_{*a}(q_s - q_z) = St_e$.

3.3. *The constraint* $Q_T = Q_S + Q_L + Q_R$

If the shear stress τ_0 in the surface layers and the geometry of the interface plus data from the measurement levels in air and water are given, then u_{*a}, u_{*w} and the various sublayer and matching level thicknesses are known because h_a^+, h_w^+, Pr_w, etc. are known. Indeed the only unknown is the interface or surface temperature T_s. For a steady-state system the fluxes must be in balance, viz.;

$$Q_T = Q_R + Q_S + Q_L. \tag{27}$$

This is an equation then for determination of T_s. The definition and results in equations (21)–(26) are introduced into equation (27) and the result is solved by simple iteration for T_s. The values of q_s and L are dependent on T_s. In the iteration the following equations are used at the air–water interface [15]:

$$q_s(\text{kg vapor/kg mixture}) = H_s/(H_s + 1), \tag{28a}$$

where the humidity (for T_s in °C):

$$H_s(\text{kg vapor/kg dry air}) = 7.077735 \times 10^{-3} - 1.95947 \times 10^{-4} T_s + 2.889 \times 10^{-5} T_s^2 \tag{28b}$$

and

$$L(\text{J/kg}) = 2.487 \times 10^6 - 2.26013 \times 10^3 T_s. \tag{29}$$

In sum equation (27) can be used to find Q_T, Q_R, Q_S, Q_L and T_s given T_∞, q_∞, T_b, u_{*a}, u_{*w}, z_∞, z_b and h. Values of Pr_a, Pr_w, Sc_a, v_a, v_w, etc. are obtained at temperatures corresponding to the surface layer values at z_b and z_z; only q_s and L are functions of T_s.

4. RELEVANT EXPERIMENTAL RESULTS

The data of Miller *et al.* [15] are used to test the theory developed in Sections 3.2 and 3.3. The measurements were made in the Stanford Wind, Water–Wave Research Facility (Fig. 2). The subset of the data used includes 26 cases of wind-generated surface roughness (water waves) with water–air temperature differences $(T_b - T_z)$ between 0° and 15 C, fetches (x) of 9.5 and 14.5 m, and water roughness Reynolds numbers (h_w^+) greater than 100 (actually free stream wind speeds of about 7 1/2 and 10 m s^{-1}). The experimental data and a few computed values from the theory are given in Table 1.

The facility is about 35 m long; the test section is approximately 20 m long, 0.9 m wide and 1.93 m high. The channel is filled with water to a depth of about 1 m, leaving a 1 m deep air flow section. Air flow is produced by a fan at the downstream end of the channel. The honeycomb situated at the end of the test section suppresses secondary flows caused by the fan. The air inlet is a curved section with a series of turning vanes, surmounted by a set of filters. An additional honeycomb and several small mesh screens straighten and condition the air flow after passage through the inlet.

In the water a beach composed of a slanting solid surface and baskets of lathe shavings minimizes wave reflections into the test section. The water is heated from below by six electric heating cables, which are located 100 mm above the channel floor and supply up to 90 kW through a temperature controller giving relatively constant air–water temperature differences (±0.2 C) over an experimental run.

An estimate $(T_s)_{EST}$ of the water surface temperature was obtained at an effective depth $z = -140\,\mu$m through use of an infrared radiometer employing an indium antimonide detector. Bulk water temperature was measured at a depth $z_b = -0.10$ m with a bead-in-glass thermistor. Extracting the bulk-temperature and surface-temperature difference estimate $\Delta T_i = T_b - (T_s)_{EST}$ involved special calibration and computational techniques and consideration of the wavelength dependent, water and air, optical properties within the detector bandwidth (1.5–5.5 μm); details are

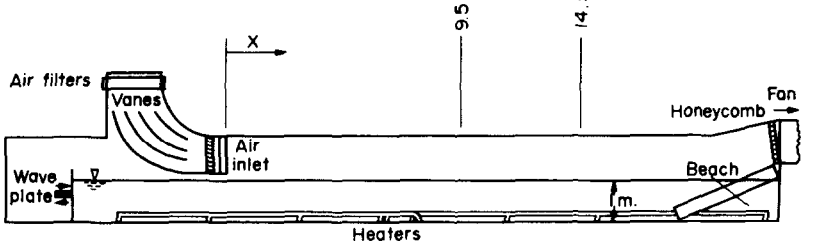

FIG. 2. Schematic of the Stanford Wind, Water–Wave Research Facility.

Table 1. Tabulated values

		Experimental Data																			Computed Values (Theory)		
Case	Station	Fetch x (m)	z_∞ (m)	z_b (m)	h (m)	U_∞ (m/s)	T_∞ (°C)	q_∞ (kg/kg)	T_b (°C)	$T_b - T_\infty$ (°C)	Pr_w	Pr_a	Sc_a	$U*_w$ (m/s)	$U*_a$ (m/s)	Q_T (W/m^2)	Q_S (W/m^2)	Q_L (W/m^2)	Q_R (W/m^2)	h^+_w	h^+_a	T_s (°C)	$T_b - T_s$ (°C)	$\frac{T_b - T_s}{T_b - T_\infty}$
1	2	14.5	0.254	-0.10	0.027	9.9	18.41	0.0081	18.61	0.20	7.2	0.71	0.60	0.0201	0.577	383	1	300	81	527	1050	18.43	0.18	0.90
2	2	14.5	0.251	-0.10	0.019	7.5	18.22	0.0081	18.57	0.35	7.2	0.71	0.60	0.0132	0.379	371	3	287	81	241	480	18.42	0.15	0.43
3	1	9.5	0.217	-0.10	0.022	10.0	19.54	0.0071	20.35	0.81	6.9	0.71	0.60	0.0204	0.587	643	18	540	85	441	841	20.11	0.24	0.30
4	1	9.5	0.206	-0.10	0.015	7.6	20.14	0.0083	22.52	2.38	6.6	0.71	0.60	0.0134	0.386	648	56	497	95	205	373	22.30	0.22	0.09
5	1	9.5	0.217	-0.10	0.022	10.0	20.49	0.0075	22.92	2.43	6.6	0.71	0.60	0.0201	0.579	851	64	691	96	459	830	22.61	0.31	0.13
6	2	14.5	0.255	-0.10	0.027	10.1	19.17	0.0076	21.65	2.48	6.6	0.71	0.60	0.0206	0.592	627	35	498	95	580	1078	21.35	0.30	0.12
7	1	9.5	0.217	-0.10	0.022	10.0	21.25	0.0066	25.78	4.53	6.2	0.71	0.60	0.0202	0.582	1159	111	938	109	493	835	25.34	0.44	0.10
8	1	9.5	0.207	-0.10	0.015	7.6	20.74	0.0063	25.68	4.94	6.2	0.71	0.60	0.0133	0.383	1003	109	784	111	218	370	25.33	0.35	0.07
9	2	14.5	0.251	-0.10	0.019	7.5	18.94	0.0081	24.60	5.66	6.4	0.71	0.60	0.0132	0.379	759	85	561	113	277	480	24.27	0.33	0.06
10	2	14.5	0.255	-0.10	0.027	10.1	19.38	0.0081	25.19	5.81	6.3	0.71	0.60	0.0206	0.592	900	90	697	114	630	1078	24.74	0.45	0.08
11	2	14.5	0.254	-0.10	0.027	9.9	20.79	0.0082	28.12	7.33	5.9	0.71	0.60	0.0200	0.576	1142	120	897	125	652	1048	27.57	0.55	0.08
12	2	14.5	0.251	-0.10	0.019	7.5	20.21	0.0090	27.58	7.37	6.0	0.71	0.60	0.0132	0.380	882	118	640	124	296	481	27.17	0.41	0.06
13	1	9.5	0.206	-0.10	0.015	7.5	22.73	0.0055	31.61	8.88	5.4	0.71	0.60	0.0132	0.381	1462	179	1146	137	246	369	31.07	0.54	0.06
14	1	9.5	0.254	-0.10	0.022	9.9	21.04	0.0054	30.43	9.39	5.6	0.71	0.60	0.0201	0.579	1699	208	1353	137	544	830	29.76	0.67	0.07
15	2	14.5	0.251	-0.10	0.019	7.5	19.21	0.0091	29.08	9.87	5.8	0.71	0.60	0.0132	0.379	952	158	657	138	307	480	28.61	0.47	0.05
16	2	14.5	0.254	-0.10	0.027	10.0	18.98	0.0081	29.27	10.29	5.7	0.71	0.60	0.0202	0.580	1282	195	947	140	677	1056	28.64	0.63	0.06
17	1	9.5	0.254	-0.10	0.022	10.1	23.67	0.0074	34.03	10.36	5.1	0.71	0.60	0.0204	0.590	1877	219	1510	148	590	845	33.29	0.74	0.07
18	1	9.5	0.206	-0.10	0.015	7.5	23.56	0.0075	34.27	10.71	5.1	0.71	0.60	0.0131	0.379	1480	195	1135	150	257	366	33.68	0.59	0.06
19	2	14.5	0.251	-0.10	0.019	7.4	17.88	0.0091	30.38	12.50	5.6	0.71	0.60	0.0130	0.372	1141	222	768	152	311	472	29.85	0.53	0.04
20	2	14.5	0.254	-0.10	0.027	10.0	18.30	0.0088	31.62	13.32	5.4	0.71	0.60	0.0204	0.585	1566	304	1105	158	717	1064	30.89	0.73	0.05
21	2	14.5	0.251	-0.10	0.019	7.5	19.47	0.0075	33.83	14.36	5.2	0.71	0.60	0.0132	0.379	1499	268	1065	166	332	480	33.15	0.68	0.05
22	1	9.5	0.206	-0.10	0.015	7.5	19.48	0.0070	34.06	14.58	5.1	0.71	0.60	0.0132	0.379	1666	285	1215	167	258	366	33.40	0.66	0.05
23	1	9.5	0.206	-0.10	0.015	7.5	22.22	0.0073	36.96	14.74	4.8	0.71	0.60	0.0131	0.378	1902	283	1446	173	271	365	36.26	0.70	0.05
24	1	9.5	0.216	-0.10	0.022	9.9	19.34	0.0070	34.19	14.85	5.1	0.71	0.60	0.0201	0.577	2122	400	1553	169	583	827	33.37	0.82	0.06
25	2	14.5	0.255	-0.10	0.027	10.1	19.67	0.0073	34.62	14.95	5.1	0.71	0.60	0.0205	0.589	2175	411	1595	170	762	1071	33.70	0.92	0.06
26	1	9.5	0.216	-0.10	0.022	9.8	21.29	0.0073	36.26	14.97	4.9	0.71	0.60	0.0198	0.570	2204	400	1630	173	599	817	35.37	0.89	0.06

given in Miller *et al.* [15]. Calibrations showed the temperature difference ΔT_i to be accurate within $\pm 0.01°C$ [yielding a possible error (at the 90% confidence level) which does not exceed 13% for the smallest ΔT_i or 0.2% for the largest ΔT_i for the data cases in Table 1].

Other parameters, such as the mean free-stream windspeed, temperature, and humidity and the water surface elevation, were obtained as well. They formed the basis for calculating the transfers Q_T, Q_S, Q_L and Q_R and surface roughness Reynolds numbers h_w^+ and h_a^+ through the use of data collected by previous investigators in the Stanford Facility (see Section 3, Mangarella *et al.* [12] and Bole and Hsu [20]). The latent and sensible heat transfers were computed from previous data; radiative heat transfer was estimated from the surface temperature measurement. The possible errors in Q_T, Q_S, Q_L, Q_R and h^+ are estimated not to exceed 14, 5, 5, 1 and 10%, respectively.

The following are key points to the present use of the data:

(1) The values of the friction velocities—the shear stress τ_0 has been measured in the facility by profile, integral and direct methods by several investigators. For the Miller *et al.* [15] study the shear stress (or friction velocity) was obtained as a function of air speed according to an equation which represents the best estimate for shear stress in the facility. Street and Miller [3] followed the concept of stress continuity, i.e. $\tau_{0_a} = \tau_{0_w}$ so:

$$u_{*_w} = (\rho_a/\rho_w)^{1/2} u_{*_a}. \tag{30}$$

This concept was used as well by Hasse [5], Saunders [4] and Kondo [8]. As Kondo points out, equation (30) implies that any stress supported by the waves is neglected. The amount of this wave stress is still under debate and pending further evidence equation (30) is used again.

(2) The value of h—Miller *et al.* [15] determined the root-mean-square (rms) of the water surface displacement $(\overline{\eta^2})^{1/2}$. Colonell [21] ran tests in the Stanford Facility and, using ocean data as well, showed that wave heights in the Laboratory and the ocean (in the absence of swell) follow a Rayleigh probability distribution to a good approximation (cf. Kinsman [22] for support of this point). From Colonell [21], then, the relationship between the mean wave height h and the rms is

$$h = (2\pi)^{1/2}(\overline{\eta^2})^{1/2} = 2.5(\overline{\eta^2})^{1/2}. \tag{31}$$

The mean wave-height h corresponds in the present cases to the mean height of roughness elements used by Yaglom and Kader [6] for solid walls.

Kondo *et al.* [23] examined the relation of high-frequency components of ocean waves to the aerodynamic roughness. They presented an examination of ocean-wave data which had been band-pass filtered in an approximate frequency range of 2–30 Hz. The lower end of their filter was not sharp and they used additional moving averages of the surface fluctuation variance to obtain a local rms scale height and "to suppress the influence of the residual low frequencies [23]". From the frequency distribution of this local scale height, they found the rms height h_p corresponding to the peak of the distribution and that the mean of the local scale height $\bar{h} \approx 2.0h_p$. In subsequent papers Kondo [8, 13] has employed h_p as the representative scale for sea-surface irregularities; however, in [8] he used the frequency range of 3–30 Hz to establish h_p. In [23] it is noted that ocean results interpreted in terms of h_p are consistent with laboratory data where the representative height is the mean height of waves with frequencies of 2–10 Hz.

It is clear that the appropriate lower frequency cutoff is not sharply defined. Kondo *et al.* [23] cite evidence that the ocean surface drag coefficient does not depend on wave components with frequencies $\leqslant 0.5$ Hz, while their data analysis in [23] leaves some doubt about the effective lower cutoff frequency for wave components. Accordingly, because of the sharp low frequency die-off from the wave energy peak in the laboratory wave spectra and because the peak energy frequency for the data used herein was always $\geqslant 2$ Hz, no filtering of the wave data of Miller *et al.* [15] was undertaken. As a consequence, while the definitions and analysis by Kondo *et al.* [23] yield $\bar{h} \sim 2(\overline{\eta^2})^{1/2}$ and consequently $h_p \sim (\overline{\eta^2})^{1/2}$, the natural relation between h and the rms displacement expressed by equation (31) is used here because the full spectrum is represented.

For data with a broader spectrum or a lower peak energy frequency (i.e. spectra with significant energy at frequencies less than 0.5–2 Hz), Kondo's approach would be appropriate. That is, for an application of the present theory, compute an $\bar{h}$ for the frequency range between 2 or 3 Hz and 30 Hz and use $\bar{h}$ in place of h in the present equations.

Miller *et al.* [15] tabulated a roughness Reynolds number $\eta_w^+ = u_{*_w}(\overline{\eta^2})^{1/2}/\nu_w$. Using equation (31) leads to:

$$h_w^+ = 2.5\eta_w^+,$$

which is given in Table 1.

(3) The nature of the surface layers—for $U_\infty > 5.0\,\mathrm{m\,s^{-1}}$ both the air and aqueous surface boundary layers are turbulent in the Stanford Facility [12, 18]. In addition the aqueous boundary-layer thickness exceeds $|z_b| = 0.10$ m; hence, the water measuring level was well within the boundary layer where logarithmic profiles were expected. For the air boundary layer, measurements of U_∞, q_∞, T_∞ were made at the edge of the boundary layer. Of course, the logarithmic region of the profile does not extend to the edge of the boundary layer; the slope of the profiles is small there and the calculations are not sensitive to the precise value of z_∞ in the air. The appropriate measurement levels for each station were determined from the Stanford data of Chambers *et al.* [14].

In the Stanford Facility the water is heated from

below by immersion heaters as noted above. The resulting unstable conditions act to destroy any mean temperature variations in the vertical except where the molecular-dominated and intermediate layers ($|z| \leqslant \delta_{T_w}$) develop properly under the forced convection of the shear- and wave-induced drift current beneath the interface. A series of rough measurements of the vertical temperature profile made in the channel under the conditions shown in Table 1 (except $T_b - T_z = 10$ C) confirms that there is no significant gradient in the bulk water zone ($|z| \geqslant \delta_{T_w}$) when the heaters are on {Arya [24] shows a similar trend for his unstable wall flows (cf., his Fig. 1 for $R_i < 0$ cases)}. On the other hand, there is a measurable gradient at low windspeeds when the heaters are off; the heaters were on for all experiments reported in this paper.

Now, the present theory assumes the existence of several flow regions in the water including (for $|z| > \delta_{T_w}$) an inertial subrange of velocity and the accompanying logarithmic temperature region (cf., Tennekes and Lumley [25]). In the Stanford Facility it is clear that a logarithmic zone of temperature variation (for $|z| > \delta_{T_w}$) does not exist in the water. Thus, in the test of the theory against Miller *et al.*'s [15] data the zone $\delta_{T_w} < |z| \leqslant |z_b|$ is deleted from the theoretical calculations to accommodate the experimental conditions; the result is that T_b is measured effectively at $|z| = \delta_{T_w}$, not at $|z| = |z_b|$. This leads to a consistent result and, because δ_{t_w} and δ_{t_w} are less than δ_{T_w}, this deletion of the zone $|z| > \delta_{T_w}$ has no effect on the analysis and use of δ_{t_w} and δ_{t_w}.

The results of Mangarella *et al.* [11, 12] clearly establish that the air surface layer is neutrally stratified and that the boundary-layer structure does feature well-established logarithmic zones for T_a, q_a, etc. Accordingly, no modification of the theory is necessary in the air.

(4) The physical constants—a large number of physical constants are used in obtaining the experimental heat and mass transfers and the theoretical results. The molecular Prandtl and Schmidt numbers are given in Table 1. The variance of these quantities in the air for the temperature range of the data was negligible. The molecular Prandtl number for water was determined as a function of the water temperature.

The densities of air and water were determined as functions of T_z and T_b, respectively. However, c_{p_w} and c_{p_a} were taken as constants. The emissivity of water $E_w = 0.97$ and the emissivity of air $E_a = 0.80$ accordingly to Miller *et al.* [15]. (Actually, it is probable that the effective $E_a \approx 1$ if radiation from the tunnel roof and walls is considered; however, even setting $Q_R \equiv 0$ changes the constant in the fundamental relation, equation (2), by less than 4%. In addition, the equation for Q_R is used, first, to generate experimental values from measured temperatures and, second, to compute Q_R values for the theory. The net effect, when theoretical and experimental comparisons are made, is an exact cancelling of that portion of the Q_R terms involving E_a. Accordingly, no correction of the Q_R data of Miller *et al.* [15] seemed worthwhile.)

The key decisions regarding parameters lie in selecting the values of Pr_{t_w}, Pr_{t_a} and Sc_{t_a}. Because of the heating from below in the water, the application of the theory was modified for data comparisons as noted above; accordingly, Pr_{t_w} does not actually enter the calculation. On the other hand, there is no data in general to suggest that Pr_{t_w} is not unity (Tennekes and Lumley [25, p. 51]); thus,

$$Pr_{t_w} = 1.0,$$

is recommended. For the air flow in the Stanford Facility there is an independent set of data reported by McIntosh *et al.* [26]. They defined dimensionless gradients Φ_H and Φ_E which for the neutrally stable cases examined here are the ratios of the eddy viscosity to the eddy diffusivities ε_H and ε_E for heat and water vapor. (Normally, in stratified flows Φ_H and Φ_E are functions of the ratio of height z to the Monin–Obukhov length L_0; for neutrally stable flows $L_0 \to \infty$.) Thus,

$$Pr_{t_a} = \frac{\varepsilon_M}{\varepsilon_H} = \Phi_H(0)$$

and

$$Sc_{t_a} = \frac{\varepsilon_M}{\varepsilon_E} = \Phi_E(0).$$

McIntosh *et al.* [26] found that $Sc_{t_a} = \Phi_E(0) = 1.19 \pm 0.08$ for pure wind-generated waves and windspeeds U_z from 3.5 to 11.0 m s^{-1}. Using $Sc_{t_a} = 1.19$ in lieu of 1.0 has a significant effect on the water vapor transfer and on the latent heat transfer. McIntosh *et al.* [26] note that the result $Sc_{t_a} = \Phi_E = 1.19$, when applied to field data obtained in the Barbados Oceanographic and Meteorological Experiment (BOMEX) by Paulson *et al.* [27], produces better agreement between direct flux and profile estimates of evaporation (Paulson *et al.* [27], use $\Phi_E = 1$).

McIntosh *et al.* [26] found that $Pr_{t_a} = \Phi_H(0)$ varied from about 0.8 to 1.4 (more or less monotically) with windspeeds U_z increasing from 3.5 to 11.0 m s^{-1}. Interestingly, while using, say, $Pr_{t_a} = 1.2$ in the present analysis does improve the comparison between theory and experiment, the improvement is slight. Thus, $Pr_{t_a} = 1.0$ has been used to obtain the results reported herein.

5. VERIFICATION OF THE THEORY

The 26 cases listed in Table 1 were used to test the theory embodied in equations (13), (14), (17)–(20), (21)–(26) and (27). This data set represents a comprehensive sample of the results of Miller *et al.* [15] for pure wind-generated waves, two fetches, water–air temperature differences from 0 to 15 C, and roughness Reynolds numbers $h^+ \geqslant 100$.

The experimental data are shown in Table 1. Because Q_R is computed according to equation (7) for both theory and experiment, no comparison is given of Q_R values. Actually, $Q_{R\,\text{EXPERIMENTAL}}$ is

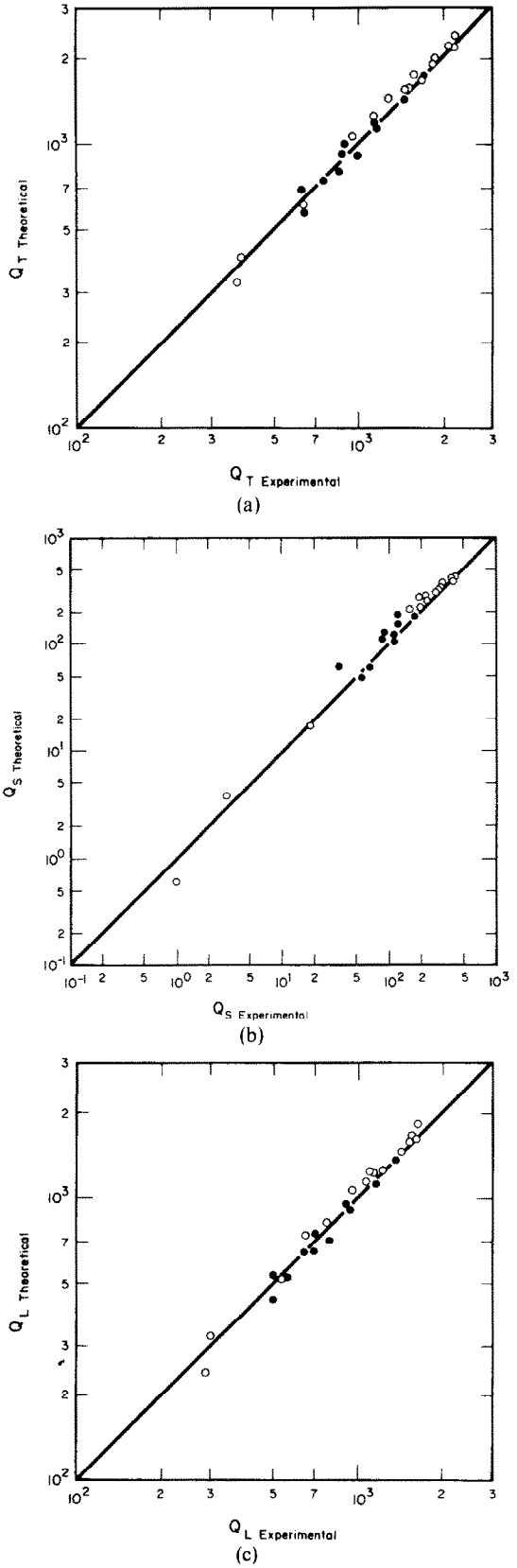

FIG. 3. Comparison of flux prediction with laboratory experimental results (solid symbols represent data cases used in [3]): (a) Total heat flux $Q_T\{\mathrm{W\,m^{-2}}\}$ in the aqueous surface layer ($Q_T = Q_S + Q_R + Q_L$); (b) Sensible heat flux $Q_S\{\mathrm{W\,m^{-2}}\}$ in the air surface layer; (c) Latent heat flux $Q_L = LQ_V\{\mathrm{W\,m^{-2}}\}$ from the interface.

computed using the radiometer measured $T_w(-140\ \mu\mathrm{m})$ while $Q_{R\,\mathrm{THEORETICAL}}$ is computed using $T_w(0) = T_s$. The difference is, of course, negligible. Figure 3 is a comparison of the predicted fluxes with those from the laboratory measurements. The results are excellent for all three flux values (Q_T, Q_S and Q_L) and clearly validate the theory. Eleven sets of the smoothed data of Mangarella, etc. (see Section 3.1) were used in [3] to establish the coefficient 0.37 in equation (2), i.e. to determine the aqueous layer heat flux which leads to an estimate of $\delta_{t_w}^+$. Those same cases are included among the 26 cases in the larger data set being used here to test the predictions of the coupled air–water theory. The eleven cases are particularly important because their aqueous layer flux is accurately predicted by the uncoupled theory of Street and Miller [3]; any significant deviation in the results for the coupled theory in these cases would represent a failure of the theory to adequately handle the air flow. The 11 cases are identified by the solid symbols in Fig. 3.

Overall, for example, the theoretical estimates of Q_T agree within $\pm 12\%$ with the experimental values which have an estimated error bound of $\pm 14\%$. This validation suggests the following. First, rough wall theory is applicable under the assumptions of steady state, negligible fetchwise gradients and constant flux surface layers and for $h^+ > 100$. Second, the relation, equation (2), established by Street and Miller [3] for the aqueous surface layer is applicable in the air surface layer as well. Third, $Sc_{t_a} = 1.19$ is an appropriate value (established independently) for the air surface boundary layer.

As a second check the theory was applied to the individual temperature and humidity profile data in the air surface layer as cited in Mangarella *et al.* [11]. There, the value of T_s was measured so the Q_S and Q_L terms can be computed directly (without iteration) from the theoretical results. The values of z_r were taken to be heights within the logarithmic variation regions for various cases as determined from the Mangarella *et al.* [11] profile data for T and q. Data for fetches of 7.7, 10.7, 12.2 and 13.8 m were used. Because the results in [11] are given in terms of Stanton numbers for heat and humidity, the predicted transfers were reduced to this form as well. Predicted total transfers were within 17% in all cases with an average error of 10% for heat transfer and 7% for water vapor (latent heat) transfer. The estimated uncertainty in the experimental data ranged from 4 to 12%.

6. AN EXAMPLE IN APPLICATION OF THE THEORY

The following example illustrates the variation of key parameters with changes in mean surface roughness (wave height) and water–air temperature difference $T_b - T_s$. The selected physical values were $u_{*a} = 0.585$ (equivalent to $U_\infty \sim 10\,\mathrm{m\,s^{-1}}$), $T_\infty = 20°\mathrm{C}$, $q_\infty = 0.0080$, $Pr_a = 0.71$, $Sc_a = 0.60$, $E_w = 0.97$, $E_a = 0.80$, $Sc_{t_a} = 1.19$, $Pr_{t_a} = 1.0$, $Pr_{t_w} = 1.0$,

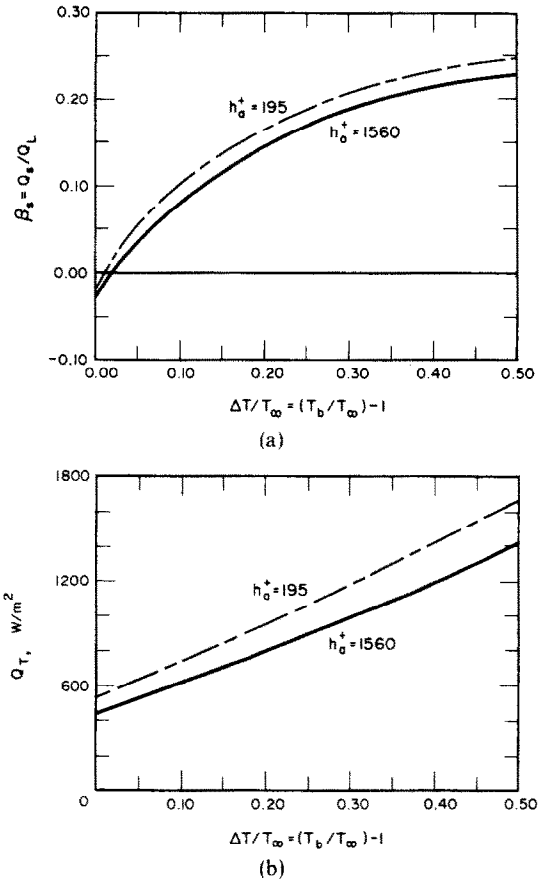

$z_\infty = 0.30$ m and, $z_b = -0.10$ m. Other values needed were calculated from these. The independent variables were h (0.005–0.040 m) and T_b (20.0 –30.0 C). The values of roughness Reynolds numbers were $100 \leqslant h_w^+ \leqslant 1020$ and $195 \leqslant h_a^+ \leqslant 1560$. The nondimensional temperature difference $(T_b - T_\infty)/T_\infty = \Delta T/T_\infty$ ranged from 0 to 0.5.

Figure 4(a) shows the variation of the so-called Bowen ratio $\beta_S = Q_S/Q_L$. It ranges from a small negative value (for the isothermal case where $T_s < T_\infty = T_b$) to the traditional values of 0.2–0.25. The effect of wave height variation is small.

Figure 4(b) shows the effects of h_a^+ and $\Delta T/T_\infty$ variations on the total transport. Notice that, while increasing $T_b - T_\infty$ increases Q_T, increasing h_a^+ decreases Q_T.

Figure 4(c) illustrates the variation of the bulk water-interface temperature difference (to which Q_T is proportional) as $\Delta T/T_\infty$ and h_a^+ are changed. Maximum values of $T_b - T_s$ occur for the highest water temperature and the largest waves. This pattern is different than that for Q_T and is caused by the behavior of the inverse transfer coefficients.

The inverse transfer coefficients or generalized resistances to transfer (inverse Stanton numbers) were defined in equations (22), (24) and (26). They are dependent on the physical characteristics of the flows, e.g. wave height, measurement levels, temperatures (as they influence Pr_w, ρ_a, ρ_w, etc.) and shear

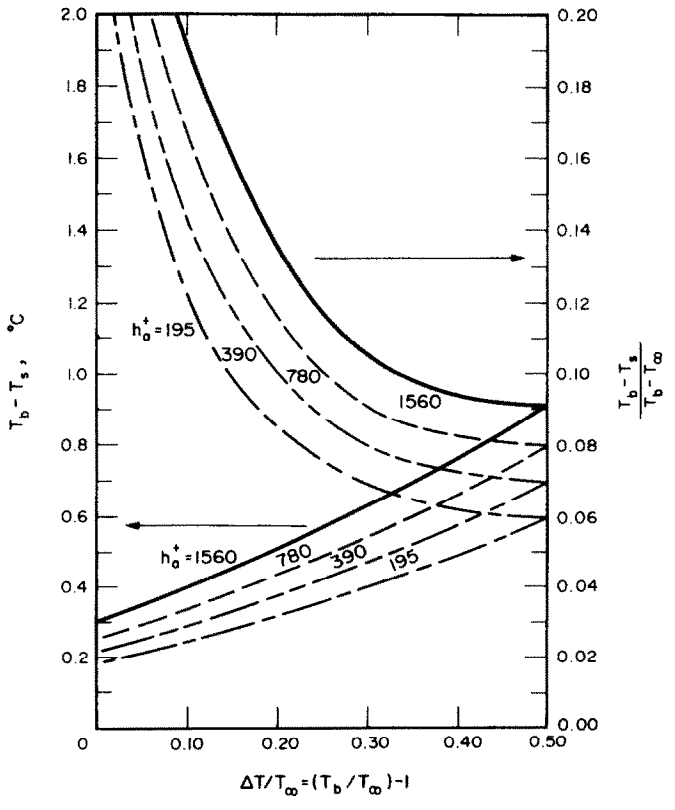

FIG. 4. Variation of parameters for illustrative case with fixed wind shear, temperature and humidity and fixed measurement points z_b and z_∞. (a) Bowen ratio; (b) Total heat transport; (c) Water–air temperature differences.

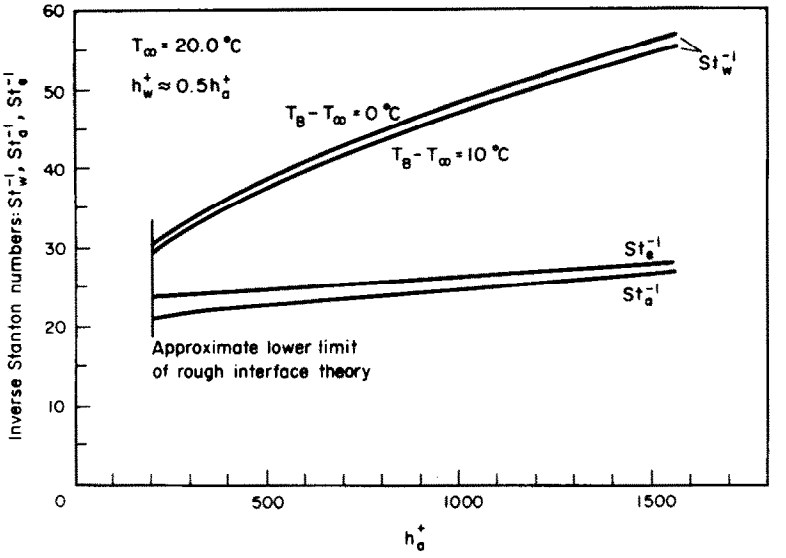

FIG. 5. Inverse Stanton numbers St_w^{-1}, St_a^{-1} and St_e^{-1} vs surface roughness for conditions of Fig. 4.

stress. Figure 5 shows how the inverse Stanton numbers St_w^{-1}, St_a^{-1} and St_e^{-1} vary with roughness Reynolds number. There is a small variation with $T_b - T_\infty$ for St_w; the others are not influenced by water temperature.

The reason for the unexpected decrease in Q_T with h_a^+ increases is now clear. The resistance to heat transfer in the water increases by over a factor of two as h_a^+ varies from 200 to 1500. Although this behavior is surprising, a hypothesis for it can be offered.

Because $Pr_w \gg 1$, the thermal sublayer thickness δ_{t_w} is about one-half of δ_{v_w}. For small h_w^+ (≈ 100 when $h_a^+ = 200$) the resistance to transfer occurs mainly from contributions for $|z| > \delta_{t_w}$. However, for $h_w^+ = 1000$ ($h_a^+ \approx 1560$) δ_{t_w} is 3.2 times larger than before, while $\delta_{T_w}^+$ is 5.6 times larger than when $h_w^+ = 100$. Accordingly, the molecular and quasimolecular (cubic variation of eddy diffusivity) zones are much more dominant at high values of h_a^+. These zones have much smaller eddy diffusivities than the turbulent zone so the resistance is higher at large roughness Reynolds numbers. Similar effects are moderated for St_a and St_e because Pr_a and Sc_a are of order one. The molecular dominated sublayers are already relatively thick. Increasing their size has then a proportionately smaller effect.

It follows from Fig. 4(b), then, that as h_a^+ goes from 195 to 1560, Q_T decreases by about 15–17%. However, from Fig. 5, it is clear that St_w^{-1} increases by over 80%. Thus, according to equation (21), in Fig. 4(c) $T_b - T_s$ and $(T_b - T_s)/(T_b - T_\infty)$ must increase with h_a^+ when $\Delta T/T_\infty$ is held constant.

Finally, $T_b - T_s$ does not exceed 1.0 C for either the experimental data set or for the example given here. One can consider ignoring the water surface layer entirely and setting $T_s = T_b$. Then an estimate for Q_R, Q_S and Q_L is obtained directly without iteration (as noted above). The sum of these gives an estimate for Q_T. As $T_b > T_s$ for the actual flow, setting $T_s = T_b$ increases Q_S, Q_L and Q_R slightly. For the cases examined herein, the overestimate of Q_T when $T_s = T_b$ is used does not exceed 8% and is usually 6% or less. This error may be acceptable in cases when accurate values of T_s and Q_S are not needed. However, this procedure is grossly in error for the prediction of T_s and Q_S when $T_b \approx T_\infty$. Then, T_s may be less than either T_b or T_∞ due to the latent heat transfer which leads to a cool film at the surface. Consequently, Q_S may be negative (i.e. transfer from the air to the water). This is seen in Fig. 4(a) for $\Delta T/T_\infty < 0.02$.

7. AN ESTIMATE OF STABILITY EFFECTS

The theory and example presented here are for neutrally stratified flow conditions. For stable or buoyant air flows the theory would need to be modified to account for the density variation effects on the eddy diffusivities in the ranges beyond the matched layers (i.e. for $z \geqslant \delta_{Q_a}$ or δ_{T_a}). Similar modification would be needed for stratified water flow. In the air, for example, empirical expressions for the dimensionless gradients Φ_H and Φ_E (see Section 4) could be introduced (cf., Dyer [28]) and the theoretical analysis completed as before. The resulting integrals might have to be evaluated numerically; however, equations (13), (17) and (19) for the sublayer thicknesses would not be altered. Equations (14), (18) and (20) would be changed because matching the cubic estimates and the outer region eddy diffusivities would bring in the stability effects.

In cases where the water surface layer flow can be ignored as indicated above, the work of Kondo [13] gives an indication of the expected effect of air surface layer stability on the generalized resistances St_a^{-1} and St_e^{-1} for rough flow. For stable cases ($T_s < T_\infty$) the effect is to reduce the transfer coefficients St_a and St_e and to increase the resistances. When the flow is unstable ($T_s > T_\infty$), the transfer coefficients

increase and the resistances decrease. For the most unstable case in the example of Section 6, i.e. for $\Delta T/T_z = 0.5$ ($T_z = 20°C$; $T_s = 30°C$), the stability effect, according to [13], is a less than 8% increase in St_a or St_e. For a hypothetical stable case using the same flow parameters but with, say, $T_z = 30$ C and $T_s = 20$ C, the estimated decrease in St_a or St_e is less than 7%. It appears, therefore, that for the high air-speeds associated with fully rough flows and for more typical temperature differences of the order of 1–3 C, forced convection is dominant and the effects of non-neutral stability are negligible.

8. CONCLUSION

The rough wall and theory presented in Sections 3.2 and 3.3 extends the work of Street and Miller [3]. The theory has been shown to be quantitatively accurate for a data set acquired in a laboratory wind, water-wave research facility. Because the sublayer thickness' relationship to surface roughness was known from [3] to be appropriate for the aqueous surface layer under rough flow conditions ($h_w^+ > 100$), the present results strongly suggest that the same relationship with the same proportionality constant is applicable in the air surface layer as well for $h_a^+ > 100$. In view of this conclusion and the direct tests (cited in Section 4) of the air surface layer portion of the coupled theory, it appears to be a rational means for predicting interface temperature and heat transfers in a turbulent, air–water interface flow situation when the interface acts as a rough boundary. The solid wall rough flow criterion of $h^+ > 100$ seems to be adequate for categorizing the regime.

Acknowledgements—This work was supported by the Atmospheric Research Section, National Science Foundation, through Grant ATM 73-06538, and by the Engineering Chemistry and Energetics Section, National Science Foundation, through Grant ENG 76-80127. The work was completed while the author was a Senior Postdoctoral Fellow at the National Center for Atmospheric Research, which is sponsored by the National Science Foundation. Many discussions with and pertinent comments from Dr. Dave McIntosh and Messrs. Bruce Howe and Stephen Klotz are gratefully acknowledged.

The author is indebted to Dr. Michel Coantic, who suggested that the eddy diffusivity variations could be examined in the context of the gas–liquid interface as defined by Davies [10], and to the referees for a number of useful suggestions.

REFERENCES

1. S. Kotake, Heat transfer and skin friction of a phase-changing interface of gas–liquid laminar flows, *Int. J. Heat Mass Transfer* **16**, 2165–2176 (1973).
2. S. Kotake, Gas–liquid laminar boundary-layer flows with a wavy phase-changing interface, *Int. J. Heat Mass Transfer* **17**, 885–897 (1974).
3. R. L. Street and A. W. Miller, Jr., Determination of the aqueous sublayer thicknesses at an air–water interface, *J. Phys. Oceanog.* **7**, 110–117 (1977).
4. P. M. Saunders, The temperature at the ocean–air interface, *J. Atmos. Sci.* **24**, 269–273 (1967).
5. L. Hasse, The sea surface temperature deviation and the heat flow at the sea–air interface, *Boundary-Layer Meteorol.* **1**, 368–379 (1971).
6. A. M. Yaglom and B. A. Kader, Heat and mass transfer between a rough wall and turbulent fluid flow at high Reynolds and Péclet numbers, *J. Fluid Mech.* **62**, 3, 601–623 (1974).
7. P. R. Owen and W. R. Thomson, Heat transfer across rough surfaces, *J. Fluid Mech.* **15**, 321–334 (1963).
8. J. Kondo, Parameterization of turbulent transport in the top meter of the ocean, *J. Phys. Oceanogr.* **6**, 712–720 (1976).
9. W. Brutsaert, A theory for local evaporation (or heat transfer) from rough and smooth surfaces at ground level, *Water Resour. Res.* **11**, 543–550 (1975).
10. J. T. Davies, *Turbulence Phenomena*. Academic Press, New York (1972).
11. P. A. Mangarella, A. J. Chambers, R. L. Street and E. Y. Hsu, Energy and mass transfer through an air–water interface, Department of Civil Engineering Technical Report No. 134, Stanford University, Stanford, California 94305 (1971).
12. P. A. Mangarella, A. J. Chambers, R. L. Street and E. Y. Hsu, Laboratory studies of evaporation and energy transfer through a wavy air–water interface, *J. Phys. Oceanogr.* **3**, 1, 93–101 (1973).
13. J. Kondo, Air–sea bulk transfer coefficients in diabatic conditions, *Boundary-Layer Meteorol.* **9**, 91–112 (1975).
14. A. J. Chambers, P. A. Mangarella, R. L. Street and E. Y. Hsu, An experimental investigation of transfer of momentum at an air–water interface, Department of Civil Engineering Technical Report No. 113, Stanford University, Stanford, California 94305 (1970).
15. A. W. Miller, Jr., R. L. Street and E. Y. Hsu, The structure of the aqueous thermal-sublayer at an air–water interface, Department of Civil Engineering Technical Report No. 195, Stanford University, Stanford, California 94305 (1975).
16. M. Coantic, Mass transfer at the ocean–air interface: small-scale hydro- and aerodynamical mechanisms, *HMT*, Pergamon Press, 1978 (in press).
17. V. G. Levich, *Physicochemical Hydrodynamics*. Prentice-Hall, Englewood Cliffs, New Jersey (1962).
18. B. M. Howe, A. J. Chambers and R. L. Street, Heat transfer at a mobile boundary, *Adv. Heat Mass Transfer at Air–Wat Interfaces, ASME*, 1–10 (1978).
19. J. Wu, Wind-induced drift currents, *J. Fluid Mech.* **68**, 49–70 (1975).
20. J. B. Bole and E. Y. Hsu, Response of gravity water waves to wind excitation, *J. Fluid Mech.* **35**, 657–676 (1969).
21. J. M. Colonell, Laboratory simulation of sea waves, Department of Civil Engineering Technical Report No. 65, Stanford University, Stanford, California 94305 (1966) [see also *J. Watways Harb. Div., Proc. Am. Soc. Civ. Engrs* **94**, WW2, 159–172 (1968)].
22. B. Kinsman, *Wind Waves*. Prentice-Hall, Englewood Cliffs, New Jersey (1965).
23. J. Kondo, Y. Fujinawa and G. Naito, High-frequency components of ocean waves and their relation to the aerodynamic roughness, *J. Phys. Oceanog.* **3**, 197–202 (1973).
24. S. P. S. Arya, Buoyancy effects in a horizontal flat-plate boundary layer, *J. Fluid Mech.* **68**, 321–343 (1975).
25. H. Tennekes and J. L. Lumley, *A First Course in Turbulence*. MIT Press, Cambridge, Massachusetts (1972).
26. D. A. McIntosh, R. L. Street and E. Y. Hsu, The influence of air–water interfacial conditions of turbulent transfer of latent and sensible heat, *Geophys. Res. Lett.* **2**, 12–14 (1975).
27. C. A. Paulson, E. Leavitt and R. Fleagle, Air–sea transfer of momentum, heat and water determined from profile measurements during BOMEX, *J. Phys. Oceanogr.* **2**, 487–497 (1972).
28. A. J. Dyer, A review of flux-profile relationships, *Boundary-Layer Meteorol.* **7**, 363–372 (1974).

TRANSFERT TURBULENT DE CHALEUR ET DE MASSE A TRAVERS UN INTERFACE RUGUEUX AIR–EAU: UNE THEORIE SIMPLE

Résumé—Le transfert résultant à travers un interface air–eau dépend du transfert de chaleur à la surface aqueuse, du rayonnement à l'interface, et des transferts de chaleur sensible et de vapeur d'eau à la surface de la couche d'air. Le problème de couplage pour ce transfert à travers l'interface sous l'action d'un écoulement d'air turbulent est résolu en appliquant une théorie pour les écoulements sur paroi rugueuse. Les prévisions théoriques et les données obtenues en laboratoire sont en bon accord. La prédiction des transferts et de la température de l'interface est faite à partir de la connaissance de la tension de frottement à l'interface, de la hauteur de rugosité, de la température et de l'humidité en un point de la couche d'air et de la température en un point de l'eau, à proximité de l'interface.

TURBULENTER WÄRME- UND STOFFÜBERGANG DURCH EINE RAUHE LUFT/WASSER-GRENZFLÄCHE. EINE EINFACHE THEORIE

Zusammenfassung—Der gesamte Transport durch eine Luft/Wasser-Grenzfläche ist abhängig vom Wärmeübergang in der wasserseitigen Grenzschicht, der Strahlung an der Phasengrenzfläche und dem Transport von fühlbarer Wärme und Wasserdampf in der luftseitigen Grenzschicht. Das gekoppelte Problem dieses Gesamttransports durch eine Phasengrenzfläche unter dem Einfluß einer turbulenten Luftströmung wird durch die Anwendung einer Theorie für Strömungen über rauhe Wände gelöst.

Theoretische Vorhersagen und Meßdaten, die an einer Laboranlage gewonnen wurden, befinden sich in zahlenmäßiger Übereinstimmung. Bei Kenntnis der Grenzflächenschubspannung und der mittleren Rauhigkeit sowie der Temperatur und Feuchte in einem Punkt in der luftseitigen Grenzschicht und der Temperatur in einem Punkt in der wasserseitigen Grenzschicht lassen sich Voraussagen über die Transportraten und die Grenzschichttemperatur machen.

ТУРБУЛЕНТНЫЙ ТЕПЛО- И МАССОПЕРЕНОС ЧЕРЕЗ ГРАНИЦУ РАЗДЕЛА ВОЗДУХ-ВОДА. ЭЛЕМЕНТАРНАЯ ТЕОРИЯ

Аннотация — Суммарный перенос через границу раздела воздух-вода зависит от переноса тепла в поверхностном слое воды, излучения на границе раздела, а также теплосодержания и переноса водяного пара в поверхностном слое воздуха. Взаимосвязанная проблема суммарного переноса через границу раздела при турбулентном течении воздуха решается с помощью теории обтекания шероховатой стенки. Получено хорошее количественное согласование результатов расчётов с экспериментальными данными. Расчёты процессов переноса и температуры границы раздела проводились в терминах касательного напряжения на границе раздела, средней высоты шероховатости стенки, а также температуры и влажности в некоторой точке в поверхностном слое воздуха и температуры в некоторой точке в поверхностном слое воды.